Ice shelf basal melting in a global finite-element sea ice – ice shelf – ocean model

R. Timmermann[1], Q. Wang[1], and H.H. Hellmer[1]

[1] *Alfred Wegener Institute for Polar and Marine Research, Bremerhaven, Germany*
E-mail: Ralph.Timmermann@awi.de

ABSTRACT. The Finite Element Sea ice Ocean Model (FESOM) has been augmented by an ice-shelf component with a three-equation system for diagnostic computation of boundary layer temperature and salinity. Ice shelf geometry and global ocean bathymetry have been derived from the RTopo-1 dataset. A global domain with a triangular mesh and a hybrid vertical coordinate is used. To evaluate sub-ice shelf circulation and melt rates for present-day climate, the model is forced with NCEP reanalysis data. Basal mass fluxes are mostly realistic with maximum melt rates in the deepest parts near the grounding lines and marine ice formation in the northern sectors of Ross Ice Shelf and Filchner-Ronne Ice Shelf. Total basal mass loss for the ten largest ice shelves reflects the importance of the Amundsen Sea ice shelves; Getz Ice Shelf is shown to be a major melt water contributor to the Southern Ocean. Despite their modest melt rates, the "cold water' ice shelves in the Weddell Sea are still substantial sinks of continental ice in Antarctica. Discrepancies between the model and observations can partly be attributed to deficiencies in the forcing data or to (sometimes unavoidable) smoothing of ice shelf and bottom topographies.

INTRODUCTION

Melting of glaciers, ice caps and ice sheets contributes to changes in global sea level. Therefore, an estimate of the rate of ice mass loss from the Antarctic Ice Sheet is an important component of the IPCC's Fifth Assessment Report. Given that most of the Antarctic Ice Sheet drains into floating glaciers or ice shelves, an understanding of sub-ice shelf processes is crucial to obtain a reliable estimate of the southern hemisphere's ice mass budget. EU project ice2sea was set up to reduce uncertainties in projections of the cryosphere's contribution to global sea level rise. The development of improved models of ocean–ice shelf interaction is an important component of this.

Modelling of processes in sub-ice shelf cavities and the quantification of ice shelf basal melt rates in an Antarctic circumpolar context go back to the Bremerhaven Regional Ice-Ocean Simulations (BRIOS) studies presented by Beckmann and others (1999), Timmermann and others (2001; 2002a,b), Assmann and others (2003), and Hellmer (2004). Although resolution in these simulations was relatively coarse and many features of ice shelf morphology and cavity topography were unknown then, a comparison with results of smaller-scale regional/local models (e.g. Gerdes et al., 1999; Grosfeld and others, 2001; Williams and others, 2001; Thoma and others, 2006; Dinniman and others, 2007) shows that BRIOS results are to a large extent realistic.

To overcome the limitations of a relatively coarse resolution and the open boundaries inherent to any regional model, and at the same time to include newly obtained information about many details of cavity geometry, we developed a finite-element sea ice-ice shelf-ocean model with a global domain, a hybrid vertical coordinate, and a horizontal mesh focussed on the Southern Ocean continental shelf including the sub-ice shelf cavities. Here, we report on the achievements in the development of this member of a new generation of ice shelf–ocean models. For validation purposes, we conducted simulations forced with NCEP reanalysis data. Sub-ice shelf circulation and melt rates for present-day climate are evaluated and compared to other model simulations (with the BRIOS model serving as one of the baseline data sets) and to observation-based estimates. We discuss the model representation of the larger ice shelves and look into possible reasons for discrepancies.

MODEL DESCRIPTION

The Finite Element Sea ice Ocean Model (FESOM; Timmermann and others, 2009) has been augmented by a newly implemented ice-shelf component. We use a three-equation system for the computation of temperature and salinity in the boundary layer between ice and ocean and the melt rate at the ice shelf base as proposed by Hellmer and Olbers (1989) and refined by Holland and Jenkins (1999). Turbulent fluxes of heat and salt are computed with coefficients depending on the friction velocity following Jenkins (1991). Like most models of ice-shelf ocean interaction, we assume a steady state for ice shelf thickness and cavity geometry; on time scales covered by the simulation, basal mass loss is assumed to be in equilibrium with surface accumulation and the divergence of the ice shelf flow field.

We use a tetrahedral mesh with a horizontal length scale of 50 km along non-Antarctic coasts, which is refined to 10 km along the Antarctic coast, 7 km under the larger ice shelves in the Ross and Weddell Seas, and to 4 km under the small ice shelves in the Amundsen Sea. While mesh size varies between 30 and 40 km in the offshore Southern Ocean, it increases to about 250-300 km in the vast basins of the Atlantic and Pacific Oceans. Model resolution is also high in some of the narrow straits that are important to the global thermohaline circulation, namely the Strait of Gibraltar, Fram and Denmark Straits, and the region between Iceland and Scotland. In total the grid comprises about 2 million grid nodes.

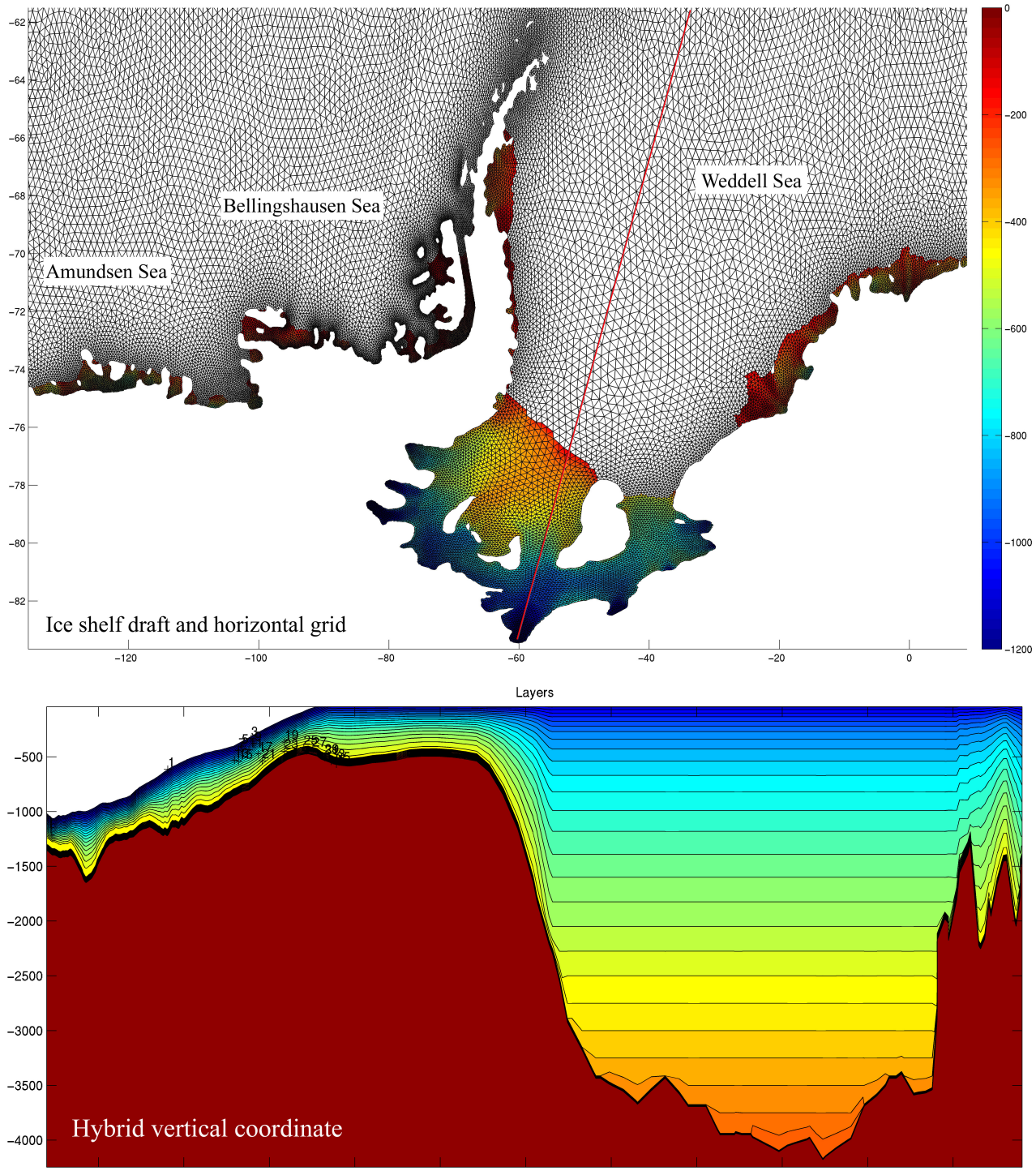

Fig. 1. Top: Ice shelf draft and horizontal grid in the Amundsen, Bellingshausen and Weddell Seas of the global model. Bottom: Vertical coordinate levels on a section from the Ronne Ice Shelf cavity to the northeast. The red line in the top panel indicates the section location.

To allow for an adequate representation of sub-ice shelf cavities and at the same time obtain a realistic global thermohaline circulation, we use a hybrid vertical coordinate system with 36 layers and a z-level discretization in the mid- and low-latitude ocean basins, while the top 23 layers use terrain-following coordinates (sigma layers) along the Antarctic coast for depths shallower than 2500 m (Fig. 1). Even in the z-coordinate region, bottom nodes are allowed to deviate from their nominal layer depth in order to facilitate a correct representation of bottom topography. Bottom elements conform to the shape of the seafloor in a way that is akin to the shaved-cells approach in finite-difference models.

Ice shelf draft, cavity geometry, and global ocean bathymetry have been derived from the RTopo-1 dataset (Timmermann and others, 2010) and thus include data from many of the most recent surveys of the Antarctic continental shelf. A Gaussian function with a width depending on the model's horizontal resolution is applied to smooth ice shelf draft and seafloor topography in the sigma-coordinate region.

For this study we force the model with daily data from the NCEP/NCAR reanalysis for the period 1958-2010. We use

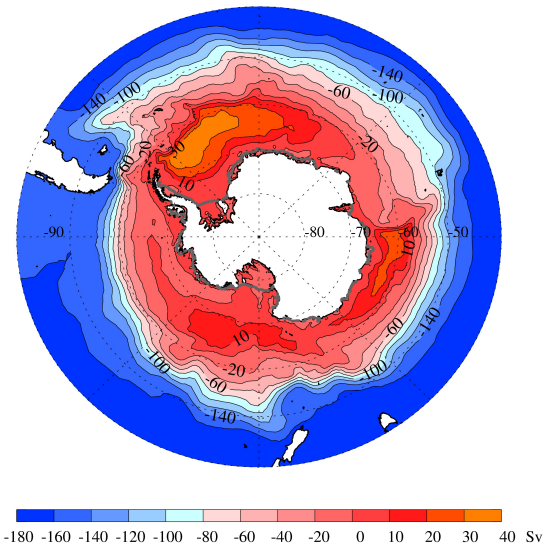

Fig. 2. Simulated mean barotropic stream function in the Southern Ocean of the global finite element sea ice–ice shelf–ocean model for the period 1980-1999.

the 10-m wind, 2-m air temperature and specific humidity, total cloudiness, and net precipitation to compute surface wind stress, turbulent sensible and latent heat fluxes, and long- and shortwave radiation. Details of the forcing strategy have been described by Timmermann and others (2009).

Initial temperature and salinity fields have been derived from NOAA's World Ocean Atlas 2001 and extended into the ice-shelf cavities using inter-/extrapolation based on minimizing the cost function

$$J(\Theta) = (d - M\Theta)(d - M\Theta)^T + (\nabla\Theta)W_\nabla(\nabla\Theta)^T \qquad (1)$$

where d represents the original data (WOA 2001 in our case), Θ is the data vector on model grid points, M is a mapping operator that projects data from the model to the atlas grid, and W_∇ represents the smoothing weights. The aim of this approach is to keep the difference between the mapped fields and the data small whereever data exist, and to minimize gradients otherwise (Sidorenko, pers. comm. 2011).

RESULTS

Ocean circulation and sea ice distribution

Like the coarse-scale FESOM simulations of Timmermann and others (2009), the model reproduces many features of ocean circulation and sea ice distribution in good agreement with observations. A map of the simulated barotropic stream function (Fig. 2) shows the three subpolar gyres with transports of 39 Sv for the Weddell Gyre, 25 Sv for the Kerguelen Gyre, and 18 Sv for the Ross Gyre. Modelled transport of the Antarctic Circumpolar Current (ACC) through Drake Passage is 150 Sv.

Simulated bottom temperatures in the Southern Ocean (Fig. 3) averaged over the period 1980-1999 agree well with data from the World Ocean Atlas 2001. High Salinity Shelf Water (HSSW) produced on the Weddell Sea continental shelf at the surface freezing point initiates the formation of Weddell Sea Deep and Bottom Water (WSDW/WSBW) that fills the deep basin of the Weddell Sea and partly spreads into

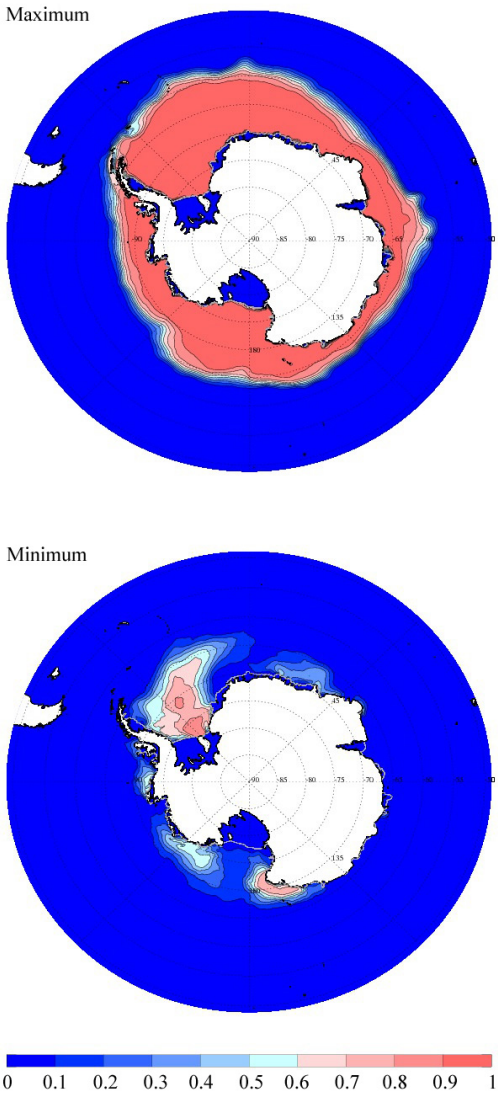

Fig. 4. Simulated mean September (top) and March (bottom) sea ice coverage in the Southern Ocean of the global finite element sea ice–ice shelf–ocean model for the period 1980-1999.

the Atlantic and Indian Oceans as Antarctic Bottom Water (AABW). Mininum temperature modelled for the central Weddell Sea basin is about −0.7°C, which compared to observations of Fahrbach and others (2011) is slightly too warm. Cold shelf waters produced in the Ross Sea leave the area with the coastal current towards Adélie Coast, so that Ross Sea Bottom Water is not replenished (at a sufficient rate) in the model.

While the temperature maximum associated with the coastal current in the Weddell Sea is reproduced well (0.3°C bottom temperature at the shelf break in the eastern/southeastern Weddell Sea), the slope front current in the Amundsen and Bellingshausen Seas is too cold by about 0.8°C. For the Amundsen Sea continental shelf (particularly in Pine Island Bay), a pronounced cold bias is evident and will be discussed later in this paper.

Compared to the experiments of Timmermann and others (2009), winter sea ice extent in our simulations is smaller and underestimates the observed maximum by about 10% (Fig. 4, top), while summer sea ice extent has increased and

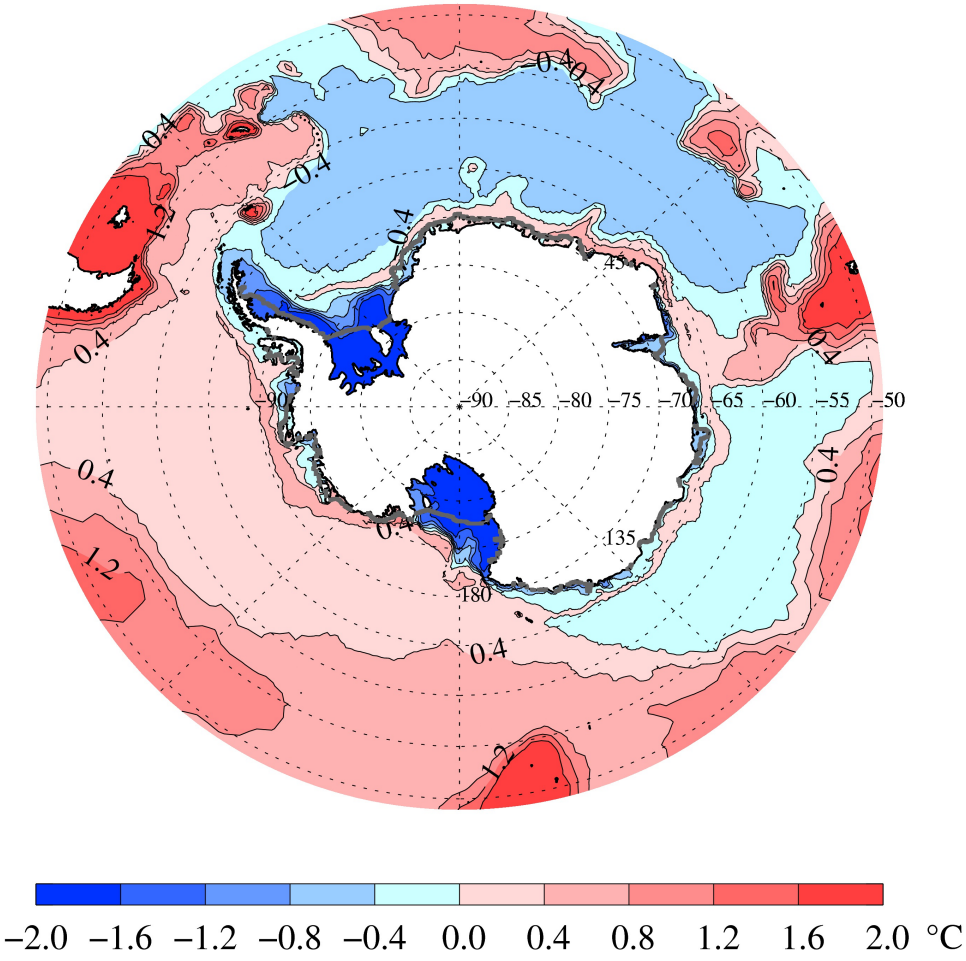

Fig. 3. Simulated mean bottom temperature in the Southern Ocean of the global finite element sea ice–ice shelf–ocean model for the period 1980-1999.

is closer to reality now. Sensitivity studies (not shown) enable us to attribute the improved summer sea ice coverage to (1) a slightly modified parameterization of lateral melting in the sea ice model and (2) to the implementation of ice shelves which (as already shown by Hellmer, 2004) cause an increase of sea ice volume by cooling and freshening the waters in the marginal seas of the Southern Ocean. For many regions, however, simulated summer sea ice concentration (Fig. 4, bottom) remains small. Contrary to observations derived from passive microwave satellite data (Cavalieri and orhers, 2006; Meier and others, 2006), the northwestern Weddell Sea (near the tip of the Antarctic Peninsula), the Amundsen Sea embayment (Pine Island Bay), and most of the East Antarctic coast are ice-free in summer in our simulations. Also summer ice coverage in the Ross Sea is underestimated. One of the topics to be discussed in the following sections is how this affects the simulation of ice shelf-ocean interaction and the estimates of basal melt rates.

Ice Shelves

Despite the fact that initial sub-ice shelf hydrography is not in equilibrium with basal heat and fresh water fluxes, ice shelf basal melt rates for most ice shelves approach a quasi-steady state within the first five years of integration (Fig. 5). Only for Filchner-Ronne Ice Shelf with its complex horizontal circulation and deep grounding line, we find a flushing (water mass replacement) time scale of about 10 years. After the initial adjustment, interannual variability is dominated by variations in summer melt rate and mostly remains within a range of ±20 %. Variability on longer (decadal) timescales is most pronounced for Getz and Ross Ice Shelves and - in contrast to year-to-year variability - determined by trends in winter melt rate. This long-term behaviour may still be part of model adjustment processes in the deep ocean, but it may also be due to a (possibly realistic) trend in the atmospheric forcing.

Melt rates from FESOM, BRIOS, and various other sources (observations and regional high-resolution models) are compiled in Table 1. Total ice shelf basal melting in FESOM is about 1600 Gt/yr; much more than in BRIOS (which had a much smaller total ice shelf area), well above the range of observation-based estimates by Jacobs and others (1996) and Rignot and Jacobs (2008), and it certainly would leave less for iceberg calving when considering present-day snow accumulation over Antarctica (about 2200 Gt/yr, e.g., according to Vaughan and others, 1999). Note though that total basal melting in FESOM includes many very small ice shelves along the coast that we decided to keep in the setup although they

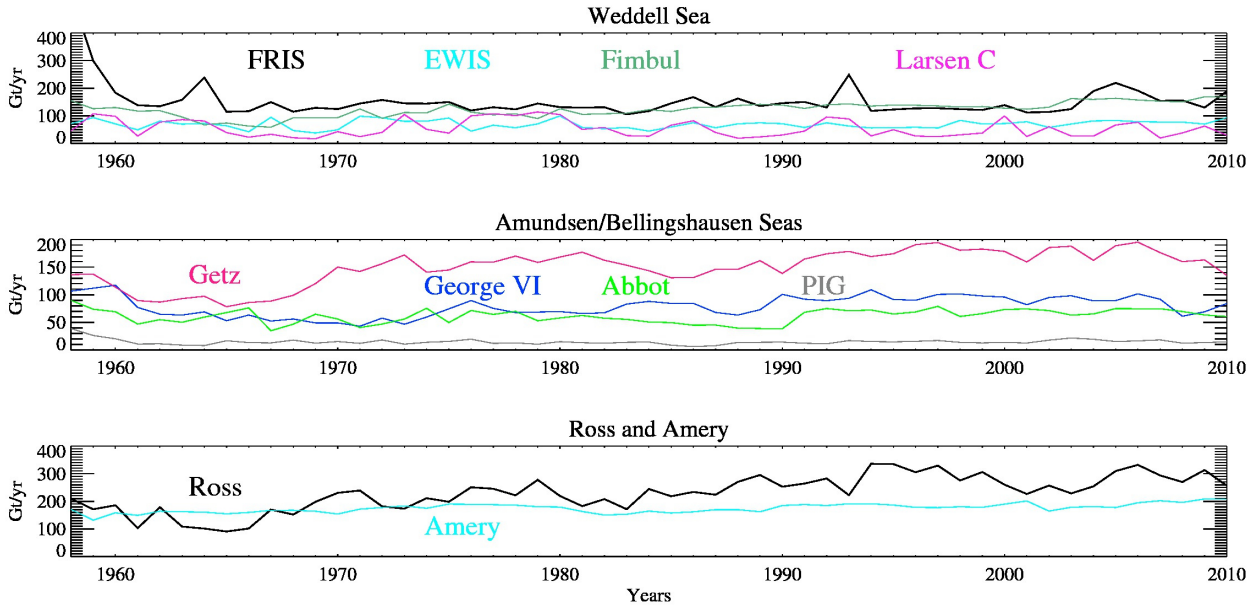

Fig. 5. Annual means of ice shelf basal mass loss (Gt/yr) for various sectors of the Southern Ocean in the FESOM hindcast simulation. Note the varying y-axis range.

are too small to have local hydrography resolved in an adequate way. Typically these floating glaciers are much more exposed to ocean heat than the larger, more secluded ice shelves; they add up to a considerable area (c.f. Table 1). In reality, these small ice shelves will lose mass mainly by calving of icebergs, while in the model they appear as areas of (substantial and apparently overestimated) basal melting.

If we only consider the sum of the ten larger ice shelves discussed in this paper, we obtain an integrated mass loss of 1130 Gt/yr. This number is in the upper range of ice shelf basal melting suggested by Jacobs et al. (1996). Some excess melting can be attributed to two particular issues rather than being a general tendency in our model simulation (see below).

Weddell Sea

Filchner-Ronne Ice Shelf

A map of basal melt rates (Fig. 6) indicates that FESOM simulates sub-ice shelf processes in good agreement with observations. Strong melting (up to 2 m/yr) occurs under Filchner Ice Shelf south of Berkner Island and particularly (up to 7 m/yr) in the deepest part of the cavity close to the grounding line, where the ice base reaches 1200 m below sea level and the *in situ* freezing point is 0.9 K below the surface freezing point.

Marine ice is formed at rates of up to 0.6 m/yr north of the Henry and Korff Ice Rises, and east of Fowler Peninsula. While the location of freezing areas is fully consistent with the observed locations of marine ice (Lambrecht and others, 2007), rates are smaller than estimates based on ice flux divergence (Joughin and Padman, 2003). Furthermore, marine ice formation in FESOM is stronger off Korff than off Henry Ice Rise, while the marine ice thickness map of Lambrecht and others (2007) suggests a stronger freezing north of Henry Ice Rise.

Two additional hot spots of marine ice formation (at rates between 0.5 and 1.0 m/yr) are associated with the outflow of Ice Shelf Water (ISW) on the western sides of the Filchner and Ronne Troughs. For the Filchner Trough, the outflow of ISW and the formation of marine ice are consistent with the sub-ice flow pattern inferred by Nicholls and others (2001) and the glaciological findings of Grosfeld and others (1998), Joughin and Padman (2003) and Lambrecht and others (2007). For Ronne Trough, evidence for marine ice formation exists for a narrow band along the coast (Nicholls and others, 2004).

A circulation regime with ISW outflow at the western side of Ronne Trough has already been proposed by BRIOS simulations for anomalously strong sea ice formation and dense water accumulation on the continental shelf north of Berkner Island (Timmermann and others, 2002b), suggesting that this may be part of a naturally occuring interannual variability. In our FESOM simulations, however, this pattern is rather persistent, which points to deficiencies in the density (salinity) distribution on the Weddell Sea's continental shelf in the model.

Area-mean net melt rate for Filchner-Ronne Ice Shelf in the FESOM simulation is 0.35 m/yr, which converts to a mass loss of about 138 Gt/yr (Table 1). These numbers are similar to the rates found in BRIOS (Hellmer, 2004) and well within the range between the estimates of Jacobs and others (1992) and Joughin and Padman (2003); they are actually close to the centre of the range suggested from hydrographic observations by Nicholls and others (2003).

The importance of tides for the patterns and magnitudes of melting and freezing in an isopycnic model of the Filchner-Ronne Ice Shelf cavity has been demonstrated by Makinson and others (2011). Even though FESOM does not consider tides, melt rate distribution and magnitudes in our simulation are much closer to their "Tidal" case than to their "Non-Tidal" simulation, and the area-mean melt rate in FESOM is considerably higher than in their "Tidal" case. We conclude that even without explicitly modelling tides, their effect can at least to some extent be covered by an appropriate choice of turbulent heat/salt exchange coefficients.

Mass Loss *melt rate* area	FESOM [this study]	BRIOS [Hellmer, 2004]	other	estimates
all	**1600 Gt/yr**	**907 Gt/yr**	**1030 Gt/yr**	[Rignot and Jacobs, 2008]
$1494{\cdot}10^3\mathrm{km}^2$	$1510{\cdot}10^3\mathrm{km}^2$	$1233{\cdot}10^3\mathrm{km}^2$		
Sum of Ten	**1130 Gt/yr**	**860 Gt/yr**	**756±380 Gt/yr**	[Jacobs and others, 1996]
$1244{\cdot}10^3\mathrm{km}^2$	$1261{\cdot}10^3\mathrm{km}^2$	$1183{\cdot}10^3\mathrm{km}^2$		
FRIS	**138 Gt/yr**	**120 Gt/yr**	**202 Gt/yr**	[Jacobs and others, 1992]
			83±25 Gt/yr	[Joughin and Padman, 2003]
	0.35 m/yr	*0.32 m/yr*	*0.55 m/yr*	[Jacobs and others, 1992]
			0.24-0.44 m/yr	[Nicholls and others, 2003]
$433 \cdot 10^3\mathrm{km}^2$	$438{\cdot}10^3\mathrm{km}^2$	$408{\cdot}10^3\mathrm{km}^2$		
Brunt + Riiser-Larsen	**65 Gt/yr**	**166 Gt/yr**		
	0.94 m/yr	*2.38 m/yr*	*0.88 m/yr*	[Thoma and others, 2006]
("EWIS")			*< 2.3 m/yr*	[Fahrbach and others, 1994]
$78.5 \cdot 10^3\mathrm{km}^2$	$77 \cdot 10^3\mathrm{km}^2$	$76 \cdot 10^3\mathrm{km}^2$		
Fimbulisen	**130 Gt/yr**	**243 Gt/yr**		
(+Jelbart)	*2.8 m/yr*	*4.91 m/yr*	*1.5-3.5 m/yr*	[Smedsrud and others, 2006]
			0.85 m/yr	[Nicholls and others, 2008]
$51.3 \cdot 10^3\mathrm{km}^2$	$53 \cdot 10^3\mathrm{km}^2$	$54 \cdot 10^3\mathrm{km}^2$		
Larsen (C)	**48 Gt/yr**	**38 Gt/yr**	**15-70 Gt/yr**	[Holland and others, 2009]
	1.0 m/yr	*0.6 m/yr*	*0.27-1.26 m/yr*	[Holland and others, 2009]
			0.35±0.19 m/yr	[Huhn and others, 2008]
$52.0 \cdot 10^3\mathrm{km}^2$	$52 \cdot 10^3\mathrm{km}^2$	$66 \cdot 10^3\mathrm{km}^2$ (B+C)		
George VI	**86 Gt/yr**	**22.5 Gt/yr**	**44 Gt/yr**	[Jacobs and others, 1992]
	3.6 m/yr	*0.43 m/yr*	*1.9 m/yr*	[Jacobs and others, 1992]
			2.1 m/yr	[Potter and Paren 1985]
			3-5 m/yr	[Jenkins and Jacobs, 2008]
$23.4 \cdot 10^3\mathrm{km}^2$	$27 \cdot 10^3\mathrm{km}^2$	$57 \cdot 10^3\mathrm{km}^2$		
Abbot IS	**59 Gt/yr**	**18 Gt/yr**	**46 Gt/yr**	[Rignot, pers. comm. 2011]
	2.1 m/yr	*0.6 m/yr*		
$31.4 \cdot 10^3\mathrm{km}^2$	$32.5 \cdot 10^3\mathrm{km}^2$	$36 \cdot 10^3\mathrm{km}^2$		
PIG	**13 Gt/yr**		**28 Gt/yr**	[Jacobs and others, 1996]
			53-85 Gt/yr	[Jacobs and others, 2011a]
	3.1 m/yr		*10 m/yr*	[Jacobs and others, 1996]
			24-50 m/yr	[Rignot, 1998]
$5.1 \cdot 10^3\mathrm{km}^2$	$5.0 \cdot 10^3\mathrm{km}^2$			
Getz IS	**164 Gt/yr**	**53.6 Gt/yr**	**128 Gt/yr**	[Jacobs and others, 2011b]
	5.4 m/yr	*1.95 m/yr*		
$35 \cdot 10^3\mathrm{km}^2$	$35 \cdot 10^3\mathrm{km}^2$	$30 \cdot 10^3\mathrm{km}^2$		
Ross IS	**260 Gt/yr**	**180 Gt/yr**	**81 Gt/yr**	[Jacobs and others, 1992]
	0.6 m/yr	*0.49 m/yr*	*0.22 m/yr*	[Jacobs and others, 1992]
			0.14 m/yr	[Dinniman and others, 2007]
$470 \cdot 10^3\mathrm{km}^2$	$475 \cdot 10^3\mathrm{km}^2$	$401 \cdot 10^3\mathrm{km}^2$		
Amery IS	**174 Gt/yr**	**18 Gt/yr**	**23 Gt/yr**	[Jacobs and others, 1996] @ $39 \cdot 10^3$ km^2
			9-18 Gt/yr	[Williams and others 1998/2001]
			30-45 Gt/yr	[Galton-Fenzi, p.c. 2011]
	2.9 m/yr	*0.35 m/yr*	*0.65 m/yr*	[Jacobs and others, 1992]
$65 \cdot 10^3\mathrm{km}^2$	$67 \cdot 10^3\mathrm{km}^2$	$55 \cdot 10^3\mathrm{km}^2$		

Table 1. Characteristics of the larger Antarctic ice shelves: Basal mass loss (bold), area-mean melt rate (italic) and ice shelf area (roman) from FESOM (average over 1980-1999), BRIOS (Hellmer, 2004), and other sources. "Sum of Ten" refers to the ten larger ice shelves considered in this study. Areas in the left column have been derived from RTopo-1 (Timmermann and others, 2010).

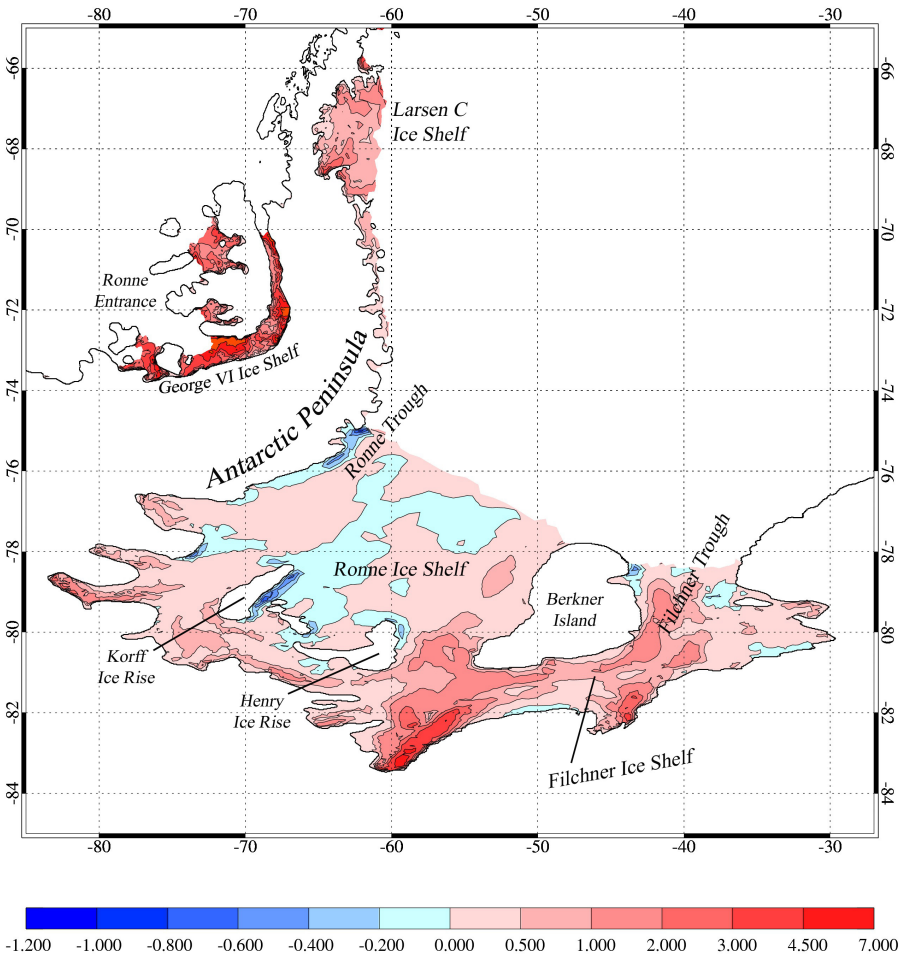

Fig. 6. Basal melt rates (m/yr) for Filchner-Ronne, Larsen C, and George VI Ice Shelves averaged over twenty years of model simulation (1980-1999). Note the non-linear color scale.

Eastern Weddell Ice Shelves

For the mean melt rate of Brunt and Riiser-Larsen Ice Shelves in the eastern Weddell Sea, Fahrbach and others (1994) suggested an upper limit of 2.3 m/yr, which is consistent with estimates from glaciological field measurements along individual flow lines (Thomas, 1973; Gjessing and Wold, 1986). BRIOS estimates even slightly exceed this upper limit (Table 1). Due to a combination of coarse resolution and strongly smoothed model topography, the warm core of the coastal current in BRIOS simulations is not well enough separated from the EWIS base, leading to spuriously high melt rates in this sector.

The improved resolution in FESOM (c.f. Fig. 1) enables us to describe this region in a much more realistic way with the coastal current being separated from the ice shelf cavities, limiting the heat available for basal melting. Basal melting in FESOM averages to 0.94 m/yr, which converts to a mass loss of 65 Gt/yr and is well within the range suggested by the regional model of Thoma and others (2006).

Fimbulisen

Similar to the case for Brunt and Riiser-Larsen Ice Shelves, and also for the same reasons, FESOM melt rates for Fimbulisen (including Jelbart Ice Shelf) are considerably smaller than in BRIOS. FESOM's mean melt rate of 2.8 m/yr (converting to a mass loss of 130 Gt/yr) is still at the upper end of the range suggested by Smedsrud and others (2006), and considerably higher than in the model simulations of Nicholls and others (2008), who use a very similar model with different boundary conditions.

Larsen Ice Shelf

Since we use the RTopo-1 ice shelf configuration, only Larsen C and a small remnant of Larsen B Ice Shelf are present in our simulation (Fig. 6). Compared to the BRIOS model, where the Larsen ice shelves were crudely approximated as 200 m thick slabs of ice, the ice draft in FESOM is more realistic; the Larsen C Ice Shelf base extends down to more than 400 m below sea level. Basal melt rates for Larsen C Ice Shelf in the FESOM simulations (48 Gt/yr mass loss, 1.0 m/yr mean melting) are therefore considerably higher than in BRIOS, from which 38 Gt/yr were obtained as a total for Larsen B and C (Table 1). Both rates are well within the range suggested by the plume model of Holland and others (2009); FESOM, however, is close to their "warm case" (temperature increased

by 0.5°C), suggesting that FESOM shelf waters in this region are slightly too warm in the annual mean.

We already mentioned the underestimation of summer sea ice extent in the northwestern Weddell Sea (Fig. 4). Reduced summer sea ice coverage is bound to cause spurious warming of surface waters, which get in touch with the northern part of Larsen C Ice Shelf and cause a strong seasonal increase of basal melting. As another consequence of this deficiency, formation of marine ice at the base of Larsen C Ice Shelf does not occur in FESOM.

Amundsen and Bellingshausen Seas

George VI Ice Shelf

For George VI Ice Shelf (Fig. 6), FESOM suggests a mean melt rate of 3.6 m/yr (mass loss of 86 Gt/yr), which is much higher than in BRIOS simulations and even exceeds the observation-based estimates of Potter and Paren (1985) and Jacobs and others (1992), but it is well within (actually at the lower end of) the range recently proposed by Jenkins and Jacobs (2008). The cavity circulation features near-bottom inflows at Ronne Entrance and in Marguerite Bay, recirculations in the northern and southern sectors of the cavity, and a northward flow along the ice shelf base into Marguerite Bay. This agrees well with the observation-based findings of Jenkins and Jacobs (2008). Modelled temperatures at the bottom of Ronne Entrance (Fig. 7) clearly show the signature of warm water originating from the Circumpolar Deep Water, but its temperature remains between 0 and 0.1 °C (Fig. 7), which is about 1°C too cold compared to observations.

Abbot Ice Shelf

Averaged basal melt for Abbot Ice Shelf in our simulation is 2.1 m/yr, corresponding to a mass loss of 58 Gt/yr, which is only slightly higher than an estimate derived from thickness and velocity measurements at the grounding line, the surface mass balance, and an approximated calving rate (Rignot, pers. comm. 2011). Sub-ice circulation features the classical cavity pattern with near-bottom inflows at Kings Peninsula and east of Thurston Island, a recirculation in the eastern basin, and outflows at the ice shelf base again at Kings Peninsula and east of Thurston Island.

Pine Island Glacier

While Jacobs and others (1996) proposed 10 m/yr mean melting (28 Gt/yr mass loss), Jacobs and others (2011a) deduced melt water fluxes of 53 km^3/yr and 85±6 km^3/yr from hydrographic observations in 1994 and 2009, respectively. Satellite-based calculations of Rignot (1998) indicate basal melting exceeding (50 ± 10) m/yr locally within the 20 km wide tidal flexure zone adjacent to the grounding line, decreasing to an average of (24 ± 4) m/yr between the hinge line and the calving front. FESOM mean melt rates near the grounding line do not exceed 7 m/yr (with the maximum melt rate located in the north-eastern corner); the total mass loss of 13 Gt/yr (corresponding to an average melt of 3.1 m/yr) is too small. The reason for the mismatch is that near-bottom water masses in FESOM's Amundsen Sea embayment are much too cold: Modelled bottom temperatures at the PIG ice front are around −0.8°C (Fig. 7), while observations show that water of ≈ 1°C has access to the interior cavity (Jenkins and others, 2010). We attribute this deficiency mainly to a cold bias in the NCEP reanalysis winter temperatures, as demonstrated by Assmann and others (2005). This cold bias induces spuriously high sea ice formation, which through excessive salt release triggers deep convection and thus an erosion of the temperature maximum associated with the Circumpolar Deep Water on the continental shelf.

Getz Ice Shelf

Recent research indicates that Getz Ice Shelf may be one of the major contributors of glacial melt water in the Southern Ocean. Based on the years 1994-2009, Jacobs and others (2011b) suggest that equilibrium basal mass loss may be as high as 80 Gt/yr, plus a disequilibrium melting of ≈ 48 Gt/yr. FESOM results propose an average basal mass loss of 164 Gt/yr, which corresponds to a mean melt rate of 5.4 m/yr. Maximum melt rates exceed 15 m/yr and are located in the troughs around Siple and Carney Islands. Water from the open ocean enters the cavity mainly (1) via a bottom-intensified inflow west of Siple Island, and (2) via a mid-depth inflow between Duncan Peninsula and Wright Island. Main outflow in our simulation occurs in the narrow passage between Siple and Carney Islands, and at the east coast of Dean Island.

Compared to hydrographic observations from *Nathaniel B. Palmer* cruise NBP0702 (Schröder, pers. comm. 2011), FESOM bottom temperatures along Getz Ice Shelf front are very close to reality west of Siple Island, while a cold bias (still related to the processes in Pine Island Bay) is evident along the eastern ice shelf front. A comparison of cross-ice-front transports to observation-based estimates still has to be done.

Ross Ice Shelf

Compared to many other ice shelves, basal melt rates for Ross Ice Shelf are rather modest. With a maximum draft of 700 m, it does not reach as far below sea level as Filcher-Ronne Ice Shelf does; maximum melt rates near the grounding line are therefore considerably lower. In FESOM, melt rates are up to 1 m/yr near the southern/southeastern grounding line (Fig. 9). Areas of marine ice formation with local maxima exceeding 1 m/yr are located in the central part of the ice shelf. This distribution of freezing and melting is similar to the BRIOS experiments and the model simulations of Dinniman and others (2007).

The twenty-year mean melt rate displayed in (Fig. 9) also features areas of strong melting along the ice front and in the areas east of Roosevelt Island and south of Ross Island. These are patterns of intense summer melting that are particularly pronounced in years with an anomalously low summer sea ice coverage. The ramp-like approximation of the ice front in FESOM and an unavoidabale smoothing of bottom topography lead to a substantial overestimation of shelf water inflow in these locations (also visible in Fig. 7). For the area east of Roosevelt Island, Hellmer and Jacobs (1995) obtained a mean basal melt rate between 0.18 and 0.27 m/yr from a two-dimensional model that had been optimized using hydrographic observations close to the ice front. This suggests that FESOM melt rates for this area are far too high.

Including the areas of spuriously high melting, mean basal mass loss is 260 Gt/yr (corresponding to a mean melt rate of 0.6 m/yr) and thus much larger than in BRIOS (180 Gt/yr, 0.49 m/yr), the estimate of Jacobs and others (1992) (81 Gt/yr, 0.22 m/yr), and the simulation of Dinniman and others (2007) (≈ 0.14 m/yr). If we compute average basal melting excluding the high-melting months December through March, Ross Ice Shelf mean melting in FESOM reduces to 172 Gt/yr (0.4 m/yr); a full 20-yr average excluding the area east and

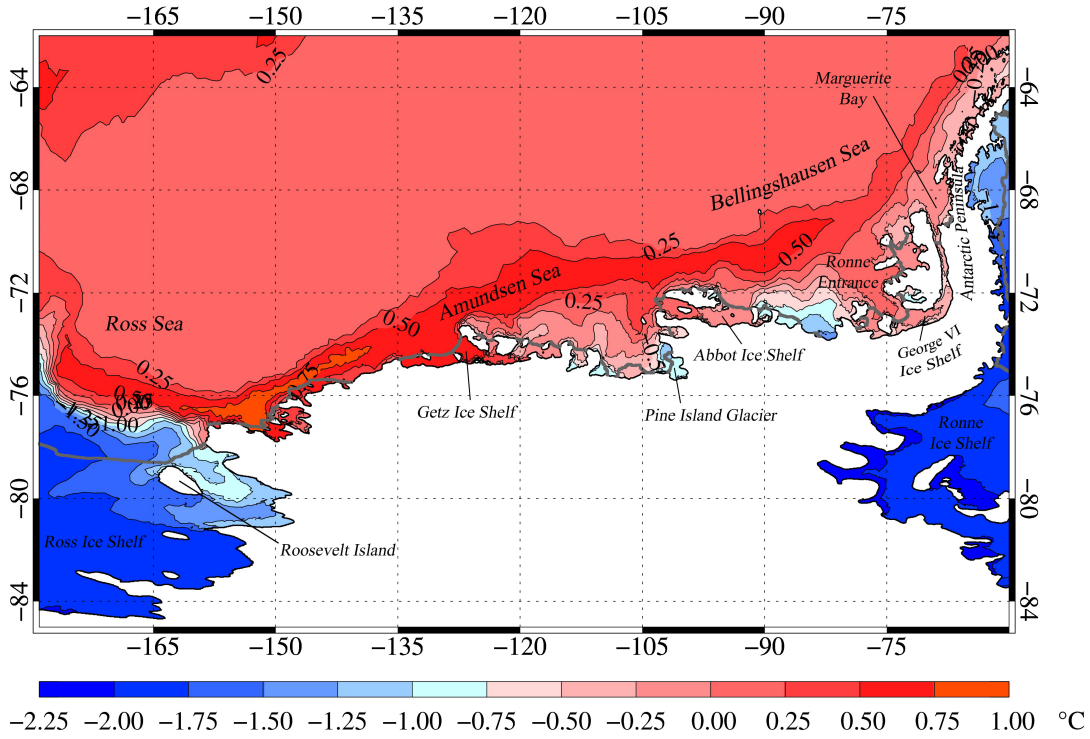

Fig. 7. Simulated bottom temperature (°C) in the Amundsen and Bellingshausen Seas, averaged over twenty years of model simulation (1980-1999).

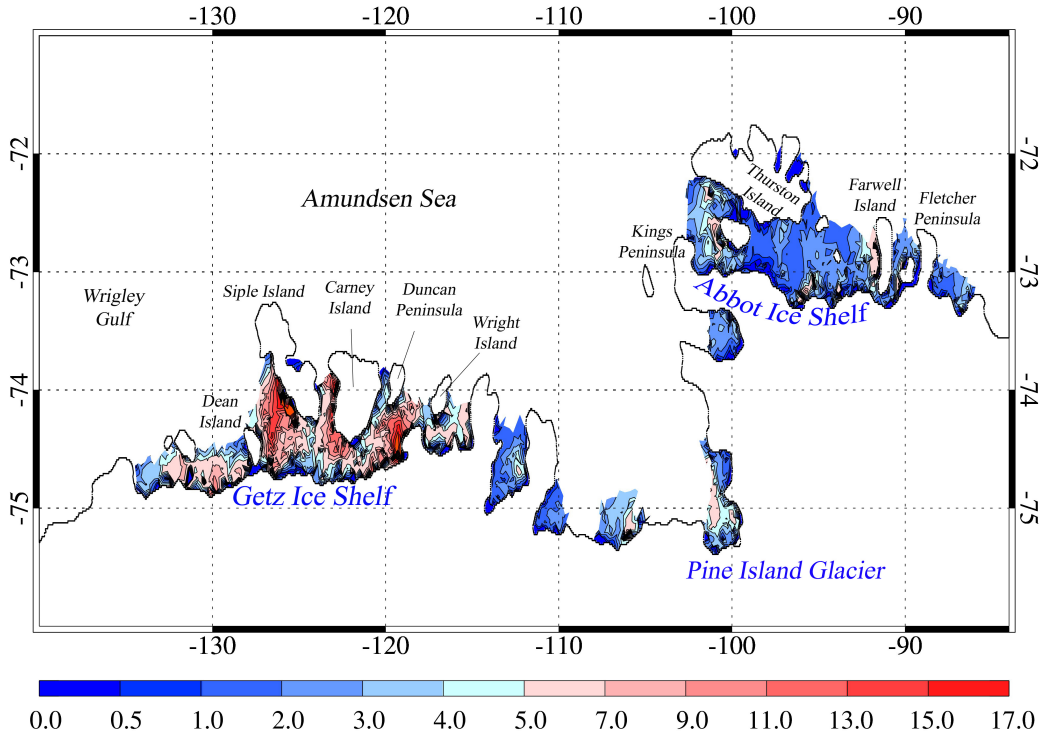

Fig. 8. Basal melt rates (m/yr) for the Amundsen Sea ice shelves, averaged over twenty years of model simulation (1980-1999). Note the non-linear color scale.

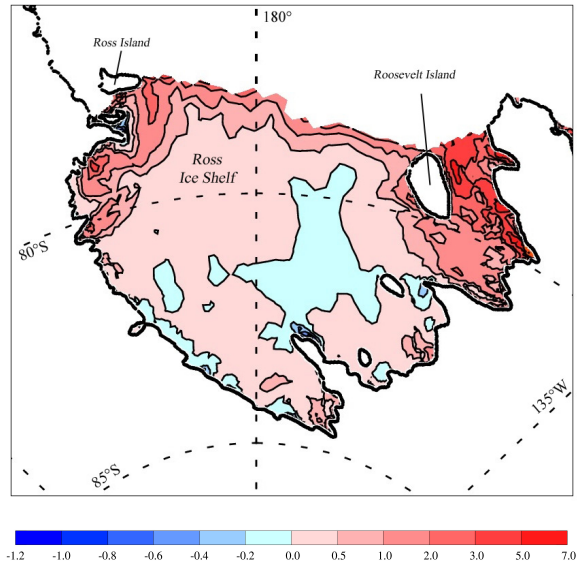

Fig. 9. Basal melt rates (m/yr) for Ross Ice Shelf averaged over twenty years of model simulation (1980-1999). Note the non-linear color scale.

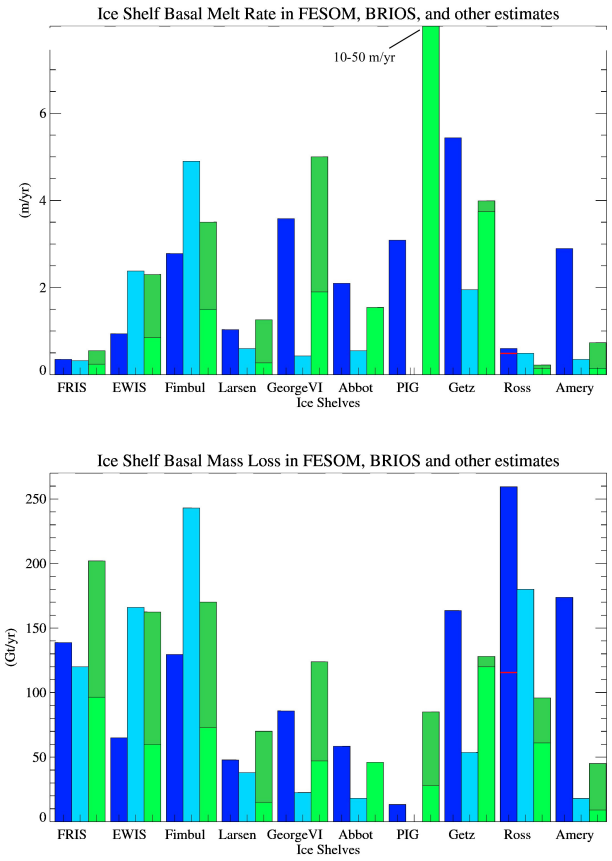

Fig. 10. Basal melt rates (m/yr, top panel) and mass loss (Gt/yr, lower panel) in FESOM (dark blue columns), BRIOS (light blue columns), and derived from independent estimates (observations or high-resolution models, green columns). The range of existing independent estimates is indicated in darker green. Note that a small range for independent estimates does not necessarily imply small uncertainties; it may also indicate the existance of only few studies (see Table 1). The red lines in the FESOM columns for Ross Ice Shelf indicate average values excluding the areas of spuriously high summer melting along the western and eastern margins of the ice shelf. Observed melt rates for PIG exceed the range of the y-axis chosen in the upper panel. References and numbers are given in Table 1.

southeast of Roosevelt Island and the area west of $168^\circ E$ (but still considering the strong melting along the ice front) yields a basal mass loss of 115 Gt/yr (mean melt rate of 0.37 m/yr), which appears much more realistic. We conclude that basal melting under large parts of Ross Ice Shelf is realistically simulated, with the exception of spuriously high melting occuring east of Roosevelt Island and south of Ross Island.

Amery Ice Shelf

Unlike the BRIOS model, the representation of Amery Ice Shelf in FESOM benefits from the ice draft and ocean bathymetry data of Galton-Fenzi and others (2008), which have been incorporated in RTopo-1. This data set is substantially improved over previous estimates of cavity geometry and features a much deeper ice draft (maximum ≈ 2500 m) and bathymetry (maximum bottom depth in the cavity $\approx$ 3000 m), while the maximum ice draft in BRIOS was only 700 m following Budd and others (1982). It is thus not surprising that melt rates calculated by FESOM are much larger than in BRIOS and also larger than the estimates of Jacobs and others (1992), who assumed an ice shelf area of only $39 \cdot 10^3$ km^2.

However, basal melting near the grounding line of Amery Ice Shelf in FESOM exceeds 20 m/yr, so that total basal mass loss amounts to 174 Gt/yr. This is much larger than any previous estimate, including results from the optimized high-resolution model of Galton-Fenzi (pers. comm., 2011) that uses the same cavity geometry (c.f. Table 1). In contrast to the Amundsen Sea embayment, where a cold bias is evident in FESOM's shelf waters, near-bottom waters in the model's Amery sector are too warm. Sensitivity studies with BRIOS (not shown) indicate that near-coast bottom temperatures in this region are very sensitive to the choice of atmospheric forcing fields and that Amery Ice Shelf basal melting may increase by a factor of ten and more in situations with too little convection on the continental shelf. We conclude that the spuriously warm shelf water in this part of the FESOM model is likely to be caused by errors in the surface forcing rather than by an overly smoothed bottom topography, although a combination of both is well possible. In any case, estimates for Amery Ice Shelf basal melting must be treated with caution.

SUMMARY, DISCUSSION AND OUTLOOK

We presented results from a global sea ice-ice shelf-ocean model based on the finite element method. The model has been used to quantify basal melt rates for the larger Antarctic ice shelves; most of them are in good agreement with observations or results from independent high-resolution models. Discrepancies can partly be attributed to deficiencies in the forcing data; possible improvements of sub-gridscale parameterizations, the representation of bottom topography / cavity geometry, and the consideration of tides are, however, still worth to be considered.

A direct comparison between BRIOS and FESOM results (Fig. 10) reveals the tendency towards higher melt rates in

places where more recent topography data suggest thicker ice, i.e. a deeper ice shelf base (e.g., Larsen C and Amery Ice Shelves). In addition, the improved resolution in FESOM enables a substantial improvement in the representation of small cavities (e.g., George VI, Abbot and Getz Ice Shelves). Where the fine resolution in FESOM allows for a better separation of the coastal current from the sub-ice shelf cavities (Fimbul, Brunt and Riiser-Larsen Ice Shelves), modelled melt rates are reduced and appear more realistic. With the exception of Amery Ice Shelf and the marginal sectors of Ross Ice Shelf, melt rates and mass loss estimates from FESOM compare well with observations and with results from independent regional high-resolution models. In this respect, the finite element approach has shown its potential and benefits to simulate processes on a horizontal scale of a few kilometers in a global model. The crucial importance of adequate atmospheric forcing has not changed, however, and neither has the challenge to obtain realistic sea ice distributions and shelf water properties in a model without flux corrections or restoring.

Further errors have been found to arise from the uncertainties in ice shelf draft and seabed topography. Although RTopo-1 includes many of the most recent surveys in this area, numbers for depth and draft are not always well constrained. An even bigger uncertainty arises from the unavoidable discretization and smoothing of topographies, especially along the ice front and the continental shelf break. Sensitivity studies (not shown) indicate that the choice of horizontal resolution and smoothing algorithms affects shelf water properties and flushing rates, and thus basal melt patterns, particularly for Getz Ice Shelf and the eastern part of Ross Ice Shelf.

Last but not least, the decision to keep the many small ice shelves along the coast in the model setup turned out to be a bad choice. The majority of these ice shelves is represented by only one line of elements, which is clearly insufficient to resolve sub-ice and ice front hydrography in an adequate way. Due to the fact that these ice shelves are typically much more exposed to ocean heat than the larger, more secluded ice shelves and that they add up to a considerable area (both in FESOM and in reality, c.f. Table 1), they are responsible for a spuriously high total ice shelf basal mass loss in the model. In reality many of these ice shelves lose mass mainly by calving of small icebergs, which melt in the marginal seas and thus provide a rather similar freshwater signal.

Our study reflects the importance of Amundsen Sea ice shelves for Antarctica's ice mass budget. Some of the highest basal melt rates are found in this drainage region for the West Antarctic Ice Sheet. Getz Ice Shelf appears as a major source of meltwater in our simulation; its contribution is roughly equal to the much larger Filchner-Ronne and Ross Ice Shelves (if we consider realistic numbers for Ross Ice Shelf melting; see the discussion of Ross Ice Shelf melt rates for details). While to date Ross and Fichner-Ronne Ice Shelves appear much less vulnerable than the "warm water" ice shelves of the Amundsen Sea, their potential fate in a warmer climate deserves further investigation.

ACKNOWLEDGEMENTS

We would like to thank K. Assmann, B. Galton-Fenzi, S.S. Jacobs, and M. Schröder for enlightening discussions, V. Haid, and D. Sidorenko for technical help and support, and the anonymous reviewers for helpful comments and suggestions. The NCEP/NCAR reanalysis data were provided by the National Oceanic and Atmospheric Administration-Cooperative Institute for Research in Environmental Sciences Climate Diagnostics Center, Boulder, online at http://www.cdc.noaa.gov. This work was supported by funding to the ice2sea programme from the European Union 7th Framework Programme, grant number 226375. This is ice2sea contribution number ice2sea42.

REFERENCES

Assmann, K., Hellmer, H. H., and Beckmann, A., 2003. Seasonal variation in circulation and water mass distribution on the Ross Sea continental shelf, *Antarctic Science*, **15(1)**, 3–11, doi:10.1017/S0954102003001007.

Beckmann, A., Hellmer, H.H., and Timmermann, R., 1999. A numerical model of the Weddell Sea: Large-scale circulation and water mass distribution, *J. Geophys. Res.*, **104(C10)**, 23375–23391.

Budd, W.F., M.J. Corry, and T.H. Jacka, 1982. Results from the Amery Ice Shelf project, *Annals of Glaciology*, **3**, 36-41.

Cavalieri, D., C. Parkinson, P. Gloersen, and H. J. Zwally, 1996, updated 2006. Sea ice concentrations from Nimbus-7 SMMR and DMSP SSM/I passive microwave data, January 1979 - June 2006. Boulder, Colorado USA: National Snow and Ice Data Center. Digital media.

Dinniman, M. S., Klinck, J. M., and Smith Jr., W. O., 2007. Influence of Sea Ice Cover and Icebergs on Circulation and Water Mass Formation in a Numerical Circulation Model of the Ross Sea, Antarctica, *J. Geophys. Res.*, **112**, C11013,doi:10.1029/2006JC004036.

Fahrbach, E., R. G. Peterson, G. Rohardt, P. Schlosser, and R. Bayer, 1994. Suppression of bottom water formation in the southeastern Weddell Sea, *Deep Sea Res.*, **41**, 389-411.

Fahrbach, E., Hoppema, M., Rohardt, G., Boebel, O., Klatt, O. and Wisotzki, A., 2011. Warming of deep and abyssal water masses along the Greenwich meridian on decadal time scales: The Weddell gyre as a heat buffer, Deep Sea Research Part II, 58 (25-26), 2509-2523, doi:10.1016/j.dsr2.2011.06.007.

Galton-Fenzi, B. K., Maraldi, C., Coleman, R., and Hunter, J., 2008. The cavity under the Amery Ice Shelf, East Antarctica, *Journal of Glaciology*, **54(188)**, 881–887.

Gerdes, R., Determann, J., and Grosfeld, K., 1999. Ocean circulation beneath Filchner-Ronne-Ice-Shelf from three-dimensional model results, *J. Geophys. Res.*, **104(C7)**, 15827–15842.

Gjessing, Y., and B. Wold, 1986. Absolut movements, mass balance and snow temperatures of the Riiser-Larsenisen, Antarctica, *Norsk Polarinstitutt, Skrifter*, **187**, 23-31.

Grosfeld, K., H. H. Hellmer, M. Jonas, H. Sandhäger, M. Schulte and D. G. Vaughan, 1998. Marine ice beneath Filchner Ice Shelf: Evidence from a multidisciplinary approach. In: *Ocean, Ice and Atmosphere: Interactions at the Continental Margin, Antarct. Res. Ser.*, **75**, edited by S. S. Jacobs , and R. F. Weiss, 319-339, AGU, Washington, D. C.

Grosfeld, K., Schröder, M., Fahrbach, E., Gerdes, R., and Mackensen, A., 2001. How iceberg calving and grounding change the circulation and hydrography in the Filchner Ice Shelf-Ocean System, *J. Geophys. Res.*, **106(C5)**, 9039–9055,doi:2000JC000601.

Hellmer, H.H., and D. Olbers, 1989. A two-dimensional model for the thermohaline circulation under an ice shelf. *Antarctic Science*, **1**, 325-336.

Hellmer, H.H, and S.S. Jacobs, 1995. Seasonal circulation unter the eastern Ross Ice Shelf, Antarctica. *J. Geophys. Res.*, **100(C6)**, 10873-10885.

Hellmer, H.H., 2004. Impact of Antarctic ice shelf basal melting on sea ice and deep ocean properties. *Geopysical Research Letters*, **31**, L10307.

Holland, D.M., and A. Jenkins, 1999. Modelling thermodynamic ice-ocean interactions at the base of an ice shelf. *J. Phys. Oceanogr.*, **29**, 1787-1800.

Holland, P. R., H. F. J. Corr, D. G. Vaughan, A. Jenkins, and P. Skvarca, 2009. Marine ice in Larsen Ice Shelf, *Geopysical Research Letters*, **36**, L11604,doi:10.1029/2009GL038162.

Huhn, O., H.H. Hellmer, M. Rhein, C. Rodehacke, W. Roether, M.P. Schodlok, and M. Schröder, 2008. Evidence of deep- and bottom-water formation in the western Weddell Sea, *Deep Sea Res.*, **55(8-9)**, 1098-1116,doi:10.1016/j.dsr2.2007.12.015.

Jacobs, S., H.H. Hellmer, C.S.M. Doake, A. Jenkins, and R.M. Frolich, 1992. Melting of ice shelves and the mass balance of Antarctica. *Journal of Glaciology*, **38(130)**, 375-387.

Jacobs, S., H. Hellmer, and A. Jenkins. 1996. Antarctic ice sheet melting in the Southeast Pacific, *Geophysical Research Letters*, **23(9)**, 957-960.

Jacobs, S., C. F. Giulivi and P. A. Mele, 2002. Freshening of the Ross Sea During the Late 20th Century, *Science*, **297(5580)**, 386-389, doi:10.1126/science.1069574.

Jacobs, S., A. Jenkins, C. Giulivi, and P. Dutrieux, 2011a. Stronger sub-ice shelf ocean circulation undermining the Pine Island Glacier, *Nature Geoscience*, **4**, 519-523, doi:10.1038/ngeo1188.

Jacobs. S., P. Dutrieux, C. Giulivi, E. Rignot, M. Schröder, S. Stammerjohn, and X. Yuan, 2011b. The Getz Ice Shelf: Antarctica's top meltwater tap? *IGS Symposium on Interaction of Ice Sheets and Glaciers with the Ocean, La Jolla*, Abstract 60A127.

Jenkins, A., 1991. A one-dimensional model of ice shelf-ocean interaction. *J. Geophys. Res.*, **96(C11)**, 20671-20677.

Jenkins, A., and S. Jacobs, 2008. Circulation and melting beneath George VI Ice Shelf, Antarctica. *J. Geophys. Res.*, **113**, C04013,doi:10.1029/2007JC004449.

Jenkins, A., P. Dutrieux, S. Jacobs, S.D. McPhail, J.R. Perrett, A.T. Webb, and D. White, 2010. Observations beneath Pine Island Glacier in West Antarctica and implications for its retreat, *Nature Geoscience*, **3**, 468–472, doi:10.1038/ngeo890.

Joughin, I., and L. Padman, 2003. Melting and freezing beneath Filchner-Ronne Ice Shelf, Antarctica, *Geopysical Research Letters*, **30(9)**, 1477,doi:10.1029/2003GL016941.

Lambrecht, A., H. Sandhäger, D.G. Vaughan, and C. Mayer, 2007. New ice thickness maps of Filchner-Ronne Ice Shelf, Antarctica, with specific focus on grounding lines and marine ice, *Antarctic Science*, **19(4)**, 521–532, doi:10.1017/S0954102007000661.

Makinson, K., P.R. Holland, A. Jenkins, K.W. Nicholls, and D.M. Holland, 2011. Influence of tides on melting and freezing beneath Filchner-Ronne Ice Shelf, Antarctica, *Geopysical Research Letters*, **38**, L06601,doi:10.1029/2010GL046462.

Meier, W., F. Fetterer, K. Knowles, M. Savoie, and M.J. Brodzik, 2006. Sea ice concentrations from Nimbus-7 SMMR and DMSP SSM/I passive microwave data. Boulder, Colorado USA: National Snow and Ice Data Center. Digital media.

Nicholls, K.W., S. Østerhus, K. Makinson, and M.R. Johnson, 2001. Oceanographic conditions south of Berkner Island, beneath Filchner-Ronne Ice Shelf, Antarctica, *J. Geophys. Res.*, **106(C6)**, 11481-11492.

Nicholls, K.W., Padman, L., Schröder, M., Woodgate, R. A., Jenkins, A., and Østerhus, S., 2003. Water mass modification over the continental shelf north of Ronne Ice Shelf, Antarctica, *J. Geophys. Res.*, **108(C8)**, 3260, doi:10.1029/2002JC001713.

Nicholls, K.W., K. Makinson and S. Østerhus, 2004. Circulation and water masses beneath the northern Ronne Ice Shelf, Antarctica, *J. Geophys. Res.*, **109**, C12017, doi:10.1029/2004JC002302.

Nicholls, K.W., E.P. Abrahamsen, K.J. Heywood, K. Stansfield, and S. Østerhus, 2008. High-latitude oceanography using the AUTOSUB autonomous underwater vehicle, *Limnology and Oceanography*, **53(5, part 2)**, 2309-2320.

Potter, J.R. and Paren, J. G., 1985. Interaction between ice shelf and ocean in George VI Sound, Antarctica, in: *Oceanology of the Antarctic Continental Shelf*, edited by: Jacobs, S., *Antarctic Research Series*, **43**, 35–58, American Geophysical Union.

Rignot, E., 1998. Fast Recession of a West Antarctic Glacier, *Science*, **281**, 549-551, doi:10.1126/science.281.5376.549.

Rignot, E., and S. Jacobs, 2008. Ice-shelf melting around Antarctica, American Geophysical Union, Fall Meeting 2008, abstract #C41D-02.

Smedsrud, L. H., Jenkins, A., Holland, D. M., and Nøst, O. A., 2006. Modeling ocean processes below Fimbulisen, *J. Geophys. Res.*, **111**, C01007,doi:10.1029/2005JC002915.

Thoma, M., Grosfeld, K., and Lange, M. A., 2006. The impact of the Eastern Weddell Ice Shelves on water masses in the eastern Weddell Sea, *J. Geophys. Res.*, **111**, C12010,doi:10.1029/2005JC003212.

Thomas, R. H., 1973. The dynamics of the Brunt Ice Shelf, Coats Land, Antarctica, *British Antarctic Survey Science Report*, **79**, Cambridge, UK.

Timmermann, R., Beckmann, A., Hellmer, H. H., 2001. The role of sea ice in the fresh water budget of the Weddell Sea, *Annals of Glaciology*, **33**, 419–424.

Timmermann, R., A. Beckmann, and H.H. Hellmer, 2002a. Simulation of ice-ocean dynamics in the Weddell Sea. Part I: Model configuration and validation, *J. Geophys. Res.*, **107(C3)**, doi:10.1029/2000JC000741.

Timmermann, R., H.H. Hellmer, and A. Beckmann, 2002b. Simulation of ice-ocean dynamics in the Weddell Sea. Part II: Interannual variability 1985 — 1993, *J. Geophys. Res.*, **107(C3)**, doi:10.1029/2000JC000742.

Timmermann, R., S. Danilov, J. Schröter, C. Böning, D. Sidorenko, and K. Rollenhagen, 2009. Ocean circulation and sea ice distribution in a finite element global sea ice – ocean model, *Ocean Modelling*, doi:10.1016/j.ocemod.2008.10.009.

Timmermann, R., A. Le Brocq, T. Deen, E. Domack, P. Dutrieux, B. Galton-Fenzi, H.H. Hellmer, A. Humbert, D. Jansen, A. Jenkins, A. Lambrecht, K. Makinson, F. Niederjasper, F. Nitsche, O.A. Noest, L.H. Smedsrud, W.H.F. Smith, 2010. A consistent dataset of Antarctic ice sheet topography, cavity geometry, and global bathymetry, *Earth System Science Data*, **2**, 261-273, doi:10.5194/essd-2-261-2010.

Vaughan, D.G., J.L. Bamber, M. Giovinetto, J. Russel, and A.P.R. Cooper, 1999. Reassessment of net surface mass balance in Antarctica. *Journal of Climate*, **12**, 933-946.

Williams, M. J. M., R.C. Warner, and W.F. Budd, 1998. The effects of ocean warming on melting and ocean circulation under the Amery ice shelf, East Antarctica, *Annals of Glaciology*, **27**, 75-80.

Williams, M. J. M., Grosfeld, K., Warner, R., Gerdes, R., and Determann, J., 2001. Ocean circulation and ice-ocean interaction beneath the Amery Ice Shelf, Antarctica, *J. Geophys. Res.*, **106(C10)**, 22383–22399.